




# *Vibrio cholerae* Motility in Aquatic and Mucus-Mimicking Environments

 Marianne Grognot,<sup>a</sup> Anisha Mittal,<sup>a</sup> Mattia Mah'moud,<sup>a</sup>  Katja M. Taute<sup>a</sup>

<sup>a</sup>Rowland Institute at Harvard, Cambridge, Massachusetts, USA

**ABSTRACT** Cholera disease is caused by *Vibrio cholerae* infecting the lining of the small intestine and results in severe diarrhea. *V. cholerae*'s swimming motility is known to play a crucial role in pathogenicity and may aid the bacteria in crossing the intestinal mucus barrier to reach sites of infection, but the exact mechanisms are unknown. The cell can be either pushed or pulled by its single polar flagellum, but there is no consensus on the resulting repertoire of motility behaviors. We use high-throughput three-dimensional (3D) bacterial tracking to observe *V. cholerae* swimming in buffer, in viscous solutions of the synthetic polymer PVP, and in mucin solutions that may mimic the host environment. We perform a statistical characterization of its motility behavior on the basis of large 3D trajectory data sets. We find that *V. cholerae* performs asymmetric run-reverse-flick motility, consisting of a sequence of a forward run, reversal, and a shorter backward run, followed by a turn by approximately 90°, called a flick, preceding the next forward run. Unlike many run-reverse-flick swimmers, *V. cholerae*'s backward runs are much shorter than its forward runs, resulting in an increased effective diffusivity. We also find that the swimming speed is not constant but subject to frequent decreases. The turning frequency in mucin matches that observed in buffer. Run-reverse-flick motility and speed fluctuations are present in all environments studied, suggesting that these behaviors also occur in natural aquatic habitats as well as the host environment.

**IMPORTANCE** Cholera disease produces vomiting and severe diarrhea and causes approximately 100,000 deaths per year worldwide. The disease is caused by the bacterium *Vibrio cholerae* colonizing the lining of the small intestine. *V. cholerae*'s ability to swim is known to increase its infectivity, but the underlying mechanisms are not known. One possibility is that swimming aids in crossing the protective mucus barrier that covers the lining of the small intestine. Our work characterizing how *V. cholerae* swims in environments that mimic properties of the host environment may advance the understanding of how motility contributes to infection.

**KEYWORDS** *Vibrio cholerae*, flagellar motility, mucin

Motility has been recognized as a major virulence factor in *V. cholerae* (1, 2), the causative agent of cholera disease, which produces severe watery diarrhea. The *V. cholerae* population recovered from the so-called "rice-water" stool of infected patients shows both stronger motility and greater infectivity than the same strain grown in the lab (3), and nonmotile *V. cholerae* mutants show decreased infectivity (4–6). The flagella that drive motility are a key target of the host immune response: flagellins trigger inflammatory responses from the host (7), and immune infant mice carry antibodies that specifically inhibit flagellum-mediated motility (8). Motility has been suggested to aid the bacteria in crossing the intestinal mucus barrier to access sites of colonization (4, 6, 9).

Despite the impact of motility on pathogenicity, characterizations of *V. cholerae*'s motility behavior have largely been qualitative, and it is commonly described as having

**Citation** Grognot M, Mittal A, Mah'moud M, Taute KM. 2021. *Vibrio cholerae* motility in aquatic and mucus-mimicking environments. *Appl Environ Microbiol* 87:e01293-21. <https://doi.org/10.1128/AEM.01293-21>.

**Editor** Gladys Alexandre, University of Tennessee at Knoxville

**Copyright** © 2021 Grognot et al. This is an open-access article distributed under the terms of the [Creative Commons Attribution 4.0 International license](https://creativecommons.org/licenses/by/4.0/).

Address correspondence to Katja M. Taute, [taute@rowland.harvard.edu](mailto:taute@rowland.harvard.edu).

**Received** 3 July 2021

**Accepted** 27 July 2021

**Accepted manuscript posted online** 4 August 2021

**Published** 28 September 2021

the appearance of “shooting stars” in dark-field microscopy (10–12). Its single polar flagellum allows the cell to swim forward or backward, being pushed or pulled by the flagellum, respectively, depending on the direction of flagellar rotation. The shorter backward swimming segments have been reported to be accompanied by random reorientation (2, 13). This description is reminiscent of the well-studied “run-tumble” motility of *Escherichia coli*, where swimming (“running”) is driven by counterclockwise (CCW) rotation of the bundled flagella, while intermittent clockwise (CW) rotation by one or more flagella breaks up the bundle and results in short reorientation events called “tumbles.” In line with this, expected motility phenotypes of chemotaxis gene deletion mutants in *V. cholerae* have often been assigned by analogy to *E. coli* (2, 13, 14). More recent work (15, 16) has described *V. cholerae*’s motility as the “run-reverse-flick” behavior reported for other polarly flagellated *Vibrio* species (17–19), where the transition from pushing to pulling is accompanied by a reversal, while the opposite transition is accompanied by a turn of approximately 90°, called a “flick.” These two views seem superficially similar but differ in their prediction for how chemotaxis, that is, the bacterium’s ability to bias its direction of motion relative to chemical gradients, can be achieved. Neither view has been supported by a full quantitative characterization of *V. cholerae*’s motility behavior.

Such a characterization, however, is crucial to understanding how motility and chemotaxis contribute to pathogenicity. The role of chemotaxis in pathogenicity is still debated (1). Butler and Camilli (2, 13) demonstrated that the infectivity of chemotaxis mutants depends on their motility phenotype, underscoring the need for an accurate, quantitative assessment of such phenotypes. Currently such an assessment is lacking even for wild-type strains.

Here, we use high-throughput three-dimensional (3D) tracking to demonstrate that *V. cholerae* performs run-reverse-flick motility with variable swimming speeds in aquatic environments and quantify the associated behavioral parameters. We show that its motility strategy of asymmetric forward and backward run durations enhances diffusive spreading. To determine whether *V. cholerae* motility behavior differs in environments that mimic physical properties of the host environment, we also observe *V. cholerae* motility in viscous polymer solutions. We show that this behavior is retained in environments that approximate the physical complexity of natural habitats.

## RESULTS

***Vibrio cholerae* performs run-reverse-flick motility in aquatic environments.** We utilize a high-throughput 3D bacterial tracking technique (20) to gather large data sets of 3D trajectories for swimming *Vibrio cholerae* O395-NT (21) (toxin deletion in classical biotype strain O395) traversing a volume spanning approximately 350  $\mu\text{m}$  in  $x$ , 300  $\mu\text{m}$  in  $y$ , and 200  $\mu\text{m}$  in  $z$ , centered approximately 135  $\mu\text{m}$  above the sample chamber’s bottom surface (Fig. 1a). We analyze 23,062 3D trajectories with an average swimming speed greater than 20  $\mu\text{m}/\text{s}$  and a duration above 1 s, culminating in 58,029 s of trajectory time, from three biological replicates. The average swimming speed in motility buffer is 94  $\mu\text{m}/\text{s}$  (Fig. 1b; see also Fig. S1 in the supplemental material).

Visual inspection of individual 3D trajectories reveals approximately straight runs, bordered by turns that alternate in magnitude, indicative of run-reverse-flick motility (Fig. 1c). We employ an automated procedure to detect turning events (see Materials and Methods). Similar to previous reports for run-reverse-flick motility in *Vibrio alginolyticus* (20) and *Caulobacter crescentus* (22), the turning angle distribution (Fig. 1d) shows two distinct peaks, one narrow peak near 180°, reflecting reversals, and a second, broader peak with a center near 90°, which we attribute to flicks.

Flicks are thought to be caused by a buckling instability of the flagellar hook that connects the flagellar filament to the flagellar motor (18). During backward swimming, the flagellum pulls the cell and the hook is likely stretched out. When the cell switches to forward swimming, the hook is compressed by the pushing flagellum and can buckle under the load if a critical force or torque threshold is reached. The buckling

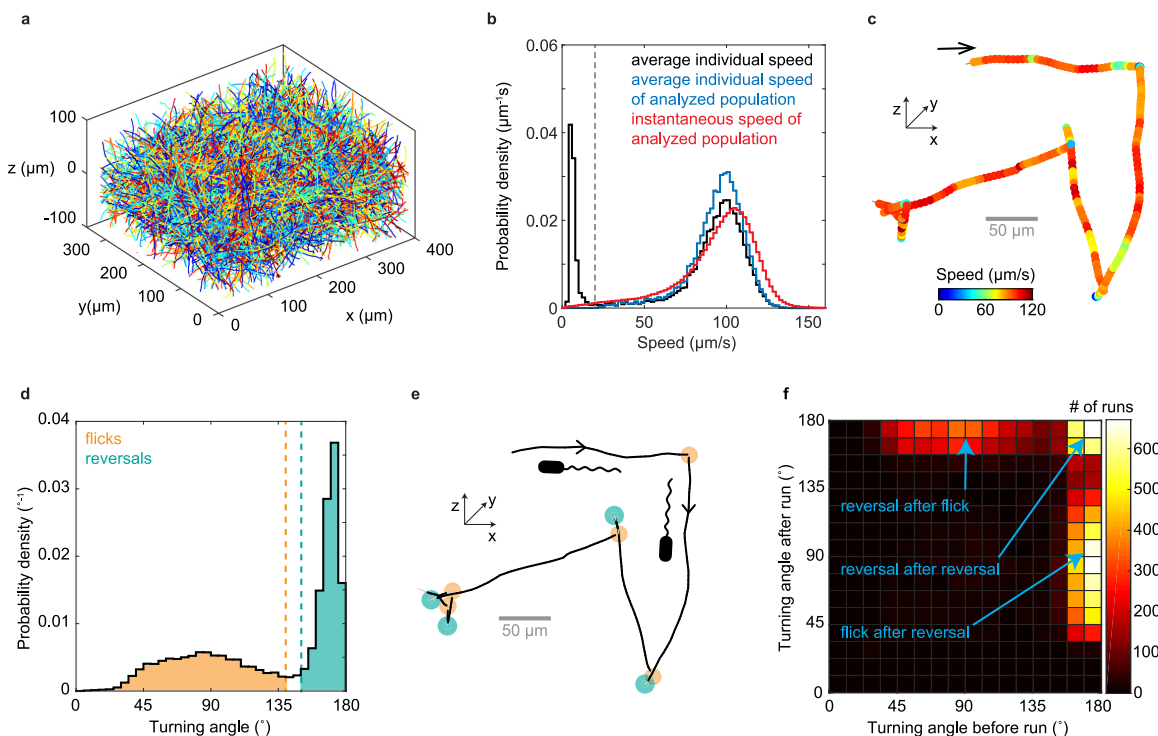


**FIG 1** *V. cholerae* 3D motility characterization. (a) 3D trajectories obtained from one 100-s-long video recording. (b) Probability distribution of average individual swimming speeds of the full population (black) and of the analyzed population (blue), weighted by trajectory duration, as well as instantaneous swimming speeds for analyzed population (red). The analyzed population consists of trajectories with an average speed larger than 20  $\mu\text{m/s}$  (marked by dashed line) and a minimal duration of 1 s. (c) Example trajectory with color reflecting swimming speed. The arrow marks the trajectory start. (d) Distribution of turning angles and classification of turn events. Turns by less than 140 $^\circ$  are considered flicks, and those by more than 150 $^\circ$  are considered reversals. Flick and reversal angles have magnitudes of  $88^\circ \pm 26^\circ$  (mean  $\pm$  SD) and  $169^\circ \pm 6^\circ$ , respectively. (e) Turn event identification in the trajectory from panel c reveals alternating flicks (orange) and reversals (teal). (f) Bivariate histogram of consecutive turning angles observed after versus before the same run. Reversals can be preceded and followed by reversals or flicks, but two flicks never occur in a row.

typically occurs within approximately 10 ms after motor reversal (18). This delay between reversal and buckling-induced reorientation is not resolved in our video rate recordings; thus, the observed flick encompasses both events. If no buckling occurs, only a reversal is observed. Thus, multiple reversals may occur in sequence. Because flicks only occur during the transition from backward to forward swimming, two flicks cannot occur in a row. To test these predictions, we analyze the magnitudes of consecutive turns (Fig. 1f) and find that reversals and flicks typically alternate. A reversal can also be followed by another reversal, but we do not observe consecutive flicks. Thus, the observed pattern of turning angle magnitudes is consistent with run-reverse-flick motility.

*V. cholerae*'s flagellar motor is driven by a sodium-motive force (23). Decreasing the sodium-motive force by decreasing the sodium concentration,  $[\text{Na}^+]$ , at constant ionic strength results in a lower swimming speed (see Fig. S1f in the supplemental material). The concomitant decrease in the occurrence of flicks (Fig. 2) is consistent with the motor torque driving the underlying buckling transition (18). Thus, we conclude that *Vibrio cholerae* performs run-reverse-flick motility.

**Forward runs are longer than backward runs.** Identifying turn events as flicks and reversals by their magnitude enables us to assign a bacterial orientation to runs without the need to visualize the flagellum. Of the 18,533 complete runs in our data set, we can identify 4,581 as forward and 8,180 as backward (see Materials and Methods). Forward runs show right-handed trajectory curvature when swimming along the bottom surface of the sample chamber, consistent with a left-handed flagellum pushing the cell by CCW rotation (24) (Fig. S2). We obtain similar average swimming speeds for

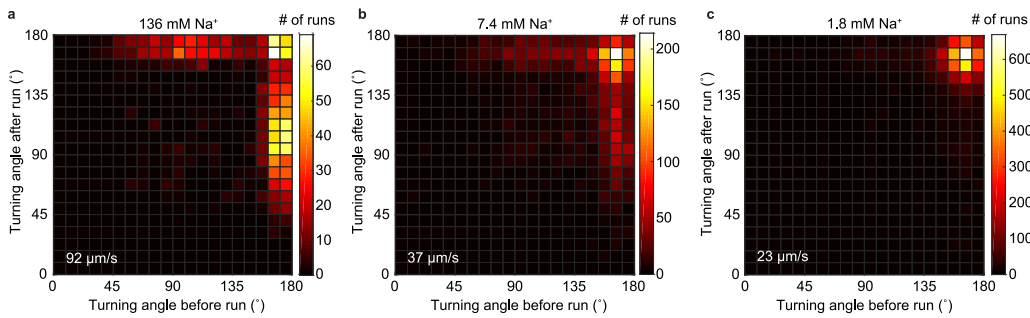


**FIG 2** *V. cholerae* flicking probability depends on the sodium motive force. Bivariate histograms of consecutive turning angles for sodium concentrations of 136 mM (a), 7.4 mM (b), and 1.8 mM (c), with respective average swimming speeds of 92, 37, and 23  $\mu\text{m/s}$ . The sodium concentration for Fig. 1f is 181 mM, and the average swimming speed is 94  $\mu\text{m/s}$ .

forward and backward runs of 90  $\mu\text{m/s}$  and 86  $\mu\text{m/s}$ , respectively. Run duration distributions for both directions show a peak at approximately 0.08 s, followed by an approximately exponential decay, which is rapid for backward runs and slow for forward runs (Fig. 3b). Peaked run duration distributions have also been found for other polarly flagellated bacteria, *Vibrio alginolyticus* (17) and *Caulobacter crescentus* (25). On average, forward runs are approximately 3.6 times longer than backward runs. While we observe no correlation in the duration of consecutive forward and backward runs (Fig. 3c), the differences in the duration of forward runs and their subsequent backward runs are exponentially distributed (Fig. 3d), with different time scales dependent on which run type is longer. One key feature of run-reverse-flick motility is that backward runs roughly retrace the preceding forward run. Given similar forward and backward run speeds, the net displacement caused by one such pair of runs is determined by their difference in durations. Exponentially distributed run duration differences have also been observed for *V. alginolyticus* (17) and, thus, may represent a common feature of species performing run-reverse-flick motility.

Run durations are expected to affect random spreading of cells (26) (Fig. 3e). The run-reverse-flick swimmers *V. alginolyticus* and *C. crescentus* show similar durations of forward and backward runs (17, 22). Theoretical work allows a prediction of the effective diffusion coefficient characterizing random spreading at long time scales (26). *V. cholerae*'s average run duration is similar to that of *V. alginolyticus*, but its asymmetry in forward and backward run durations is expected to yield an 85% increase in the diffusion coefficient compared to a symmetric scenario with the same average run duration (Fig. 3e; see also Note S1 in the supplemental material). The diffusion coefficient is also enhanced by 19% compared to a scenario where both run durations equal the longer, forward run duration. Thus, we conclude that *V. cholerae*'s asymmetric run durations enhance random spreading of cells.

**Run speed modulation.** We observe that the swimming speed during run segments is not constant but subject to substantial, temporary decreases that are readily apparent by visual inspection of trajectories (Fig. 4a). During these events, the bacterium maintains its previous swimming direction (Fig. 4b) but follows it at a decreased speed. We employ an automated detection procedure that identifies these deceleration events as decreases in speed below a threshold that lasts for at least two consecutive frames. The speed threshold is set at a fixed fraction  $\beta$  of a run-specific baseline value (see Materials and Methods), and we only consider runs with a minimum duration of 10 frames (0.33 s) to ensure that a baseline speed value can be confidently assigned. Although we consider runs of either orientation in the analysis, the runs that meet the duration threshold are likely primarily forward runs. At the selected value of  $\beta = 0.75$ , we obtain a deceleration event frequency of 0.53 Hz during runs (see Materials and Methods). While their frequency is similar to the turning frequency, we

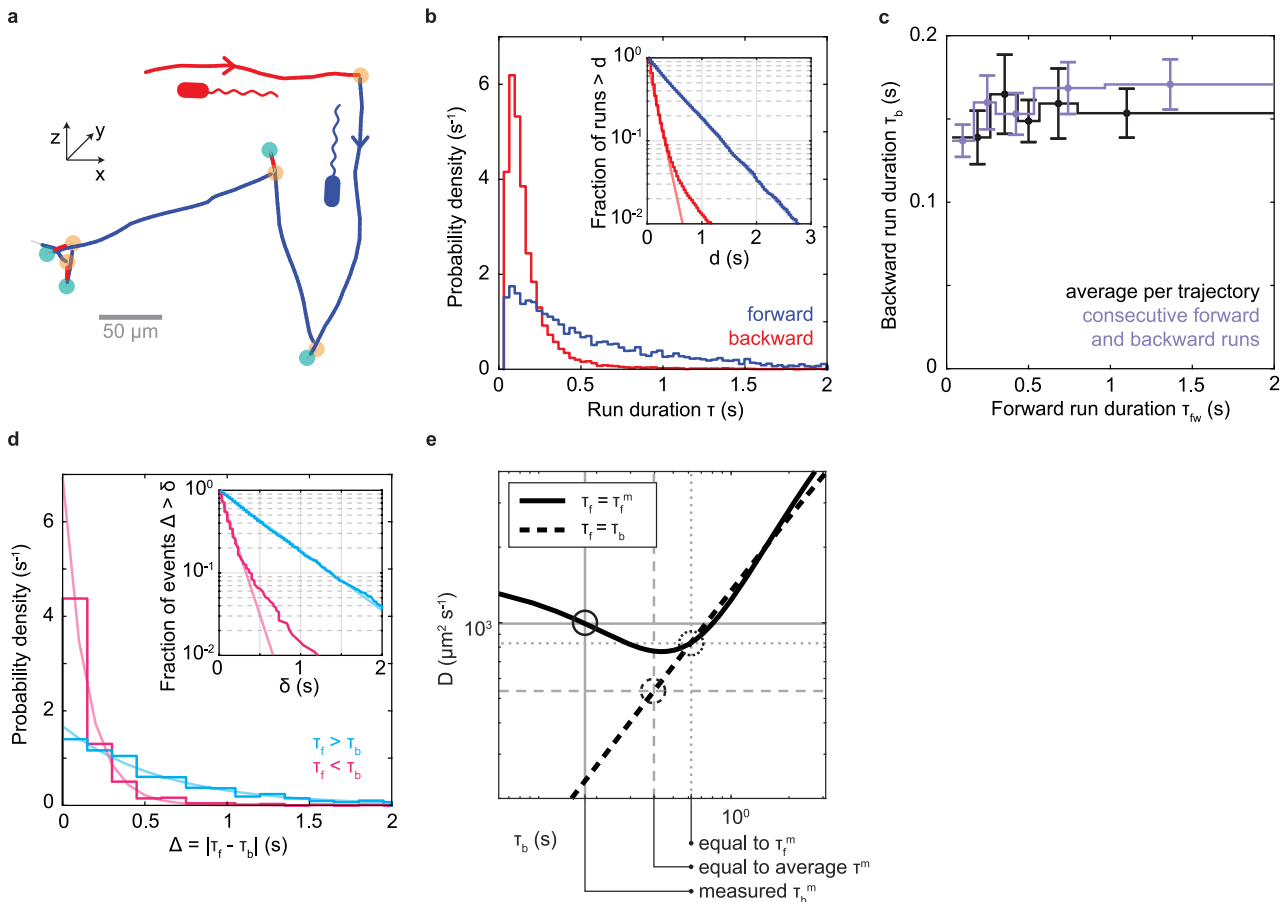


**FIG 3** Run characterization. (a) Example trajectory from Fig. 1c with runs identified as forward (blue) or backward (red) based on the identity of the bordering turning events (orange, flicks; teal, reversals). (b) Run duration distributions. Average durations of backward (red) and forward (blue) runs are  $0.174 \pm 0.002$  s (mean  $\pm$  SE) and  $0.62 \pm 0.01$  s, respectively. (Inset) Fraction of runs that are longer than a threshold,  $d$ , as a function of  $d$ . Line fits in log-linear space to the ranges of 0.1 to 1.5 s and 0.067 to 0.4 s yield exponential decay time scales of 0.60 s and 0.14 s for forward and backward runs, respectively. The tail of the backward run duration distribution likely represents misidentified forward runs. (c) Relationship between backward and forward run duration. Purple, average duration of backward runs as a function of the preceding forward run's duration; black, average duration of backward runs as a function of average duration of forward runs for trajectories containing at least 4 runs of known orientation. (d) Distribution of the absolute differences in duration between a forward run and the subsequent backward run, shown in cyan (magenta) when the forward run is longer (shorter) than the backward. (Inset) Fraction of events that are longer than a threshold,  $x$ , as a function of  $x$ . Partially transparent lines indicate exponential decay fits. For positive differences (cyan), a maximum likelihood fit of an exponential distribution yields an exponential decay time of 0.60 s. For negative differences (magenta), the slope of a line fit in semilog space in the range of 0 to 0.8 s yields a decay time of 0.14 s. We attribute the tail of the distribution for negative differences to misidentified forward runs, as in panel b. (e) Predicted effective diffusion coefficient for run-reverse-flick motility as a function of the average backward run duration,  $\tau_b$ , based on results of Taktikos et al. (26) (see Note S1 for details). The black solid line indicates a fixed forward run duration equal to the measured value,  $\tau_f = \tau_f^m = 0.62$  s, and the black dashed line indicates equal forward and backward run durations. Gray dashed lines mark a scenario where both forward and backward run durations are equal to the average measured run duration. Gray dotted lines mark the scenario where both equal the measured forward run duration. Gray solid lines indicate the measured scenario of  $\tau_f^m = 0.62$  s and  $\tau_b^m = 0.174$  s.

detect no strong correlation between estimates of the deceleration frequency and the turning frequency obtained for individual bacteria (Fig. S4f). The durations of the deceleration events are exponentially distributed (Fig. 4c), with an average duration of 0.12 s, suggesting that escape from these events is a random event with a fixed rate of occurrence. The intervals between decelerations, however, show a peaked distribution with a maximum at 0.12 to 0.15 s, followed by an exponential tail (Fig. 4d).

To determine whether these drops in speed represent discrete events or a continuous variation in speed, we examine the dependence of their properties on the event detection threshold. Their frequency, duration, and relative speed distributions vary continuously with the threshold parameter,  $\beta$  (Fig. S4c, e to f), suggesting that they derive from a continuous variation in speed. The ratio of variances of instantaneous and trajectory-averaged speeds of the analyzed population provides an upper limit on

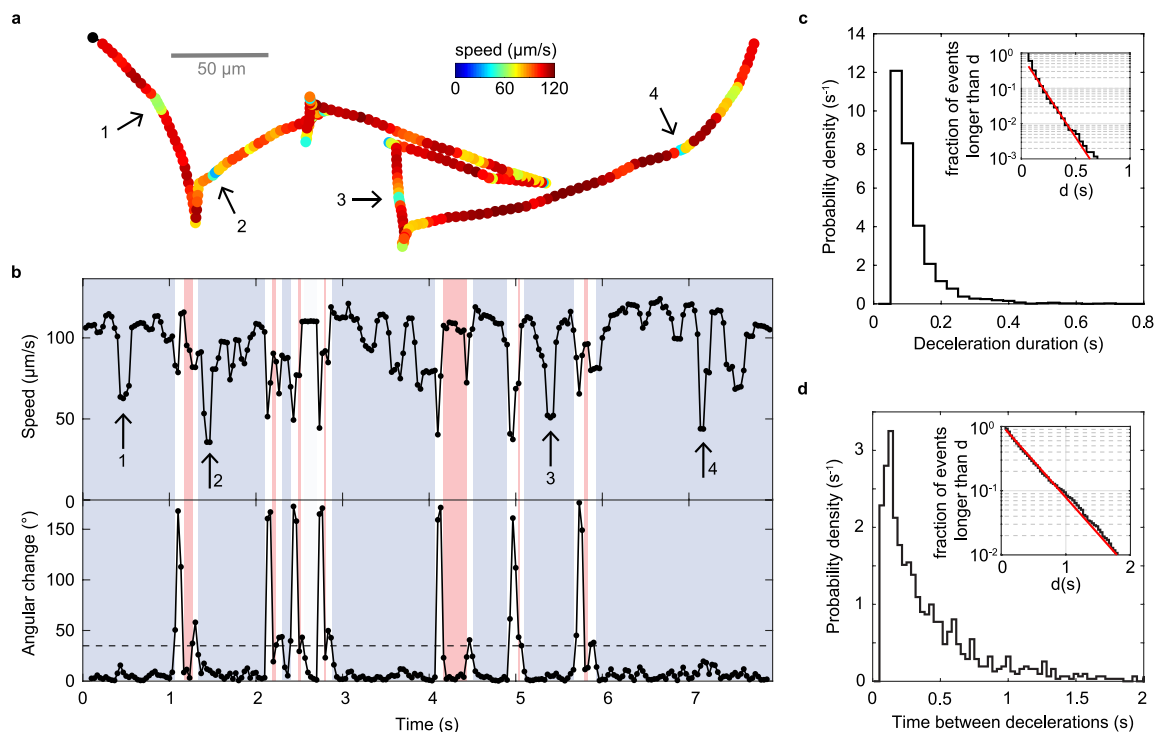


**FIG 4** Deceleration events. (a) Example trajectory with visually apparent segments of decreased speed marked by arrows. (b) Time series of swimming speed (top) and angular change in swimming direction between consecutive frames (bottom) for the trajectory shown in panel a. Blue segments represent forward swimming, red segments backward swimming. (c) Distribution of durations of deceleration events. The average duration is 0.12 s. (Inset) Fraction of events longer than a threshold,  $d$ , as a function of  $d$ . The slope of a linear fit (red) in semilog space yields an exponential decay time of 0.094 s. (d) Distribution of time between two consecutive decelerations. The average is 0.41 s. (Inset) Fraction of events longer than a threshold,  $d$ , as a function of  $d$ . The slope of a linear fit (red) in the range of 0.16 to 2 s in semilog space yields an exponential decay time constant of 0.38 s.

the contribution of interindividual, as opposed to temporal, variability at the population level. Based on the standard deviations of 24  $\mu\text{m/s}$  and 17  $\mu\text{m/s}$  observed for their respective distributions, we conclude that at least half the variability in speed observed at the population level derives from such temporal, intraindividual variability.

Errors in the bacterial position determination can produce fluctuations in the measured velocity if the magnitude of the errors is comparable to the true displacement between neighboring frames. The errors on the measured speed are thus larger for slower-swimming bacteria. To rule out measurement errors as the source of the observed speed fluctuations, we acquire trajectories for another run-reverse-flick swimmer with a lower swimming speed, *Caulobacter crescentus*, under the same measurement conditions. We find that the relative variation in run speed is larger for *V. cholerae* than for *C. crescentus* (Fig. S4g) and, thus, rule out measurement errors as the cause of the speed variations observed in *V. cholerae*. We also confirm that deceleration events are not caused by our trajectory filtering method (Fig. S4a and b).

**Run-reverse-flick motility in mucin solutions.** Run-reverse-flick motility has been viewed as an adaptation to marine habitats (27), raising the question of whether this behavior is preserved in environments as physically complex as the host environment, where the bacteria have to cross a viscous mucus barrier that protects the intestinal epithelium to reach sites of infection.

The primary component of mucus is mucins, large glycoproteins that form a hydrogel with an estimated physiological concentration range of 1 to 5% (28). We track *V. cholerae* swimming in solutions of 1.2% mucin purified from human saliva. Run-reverse-flick motility is still readily apparent from the trajectories (Fig. 5a). We analyze 2,327 3D trajectories of at least 1-s duration and 20  $\mu\text{m/s}$  average speed. The swimming speed has decreased to 57  $\mu\text{m/s}$  (Fig. 5b). The bivariate distribution of turn angle

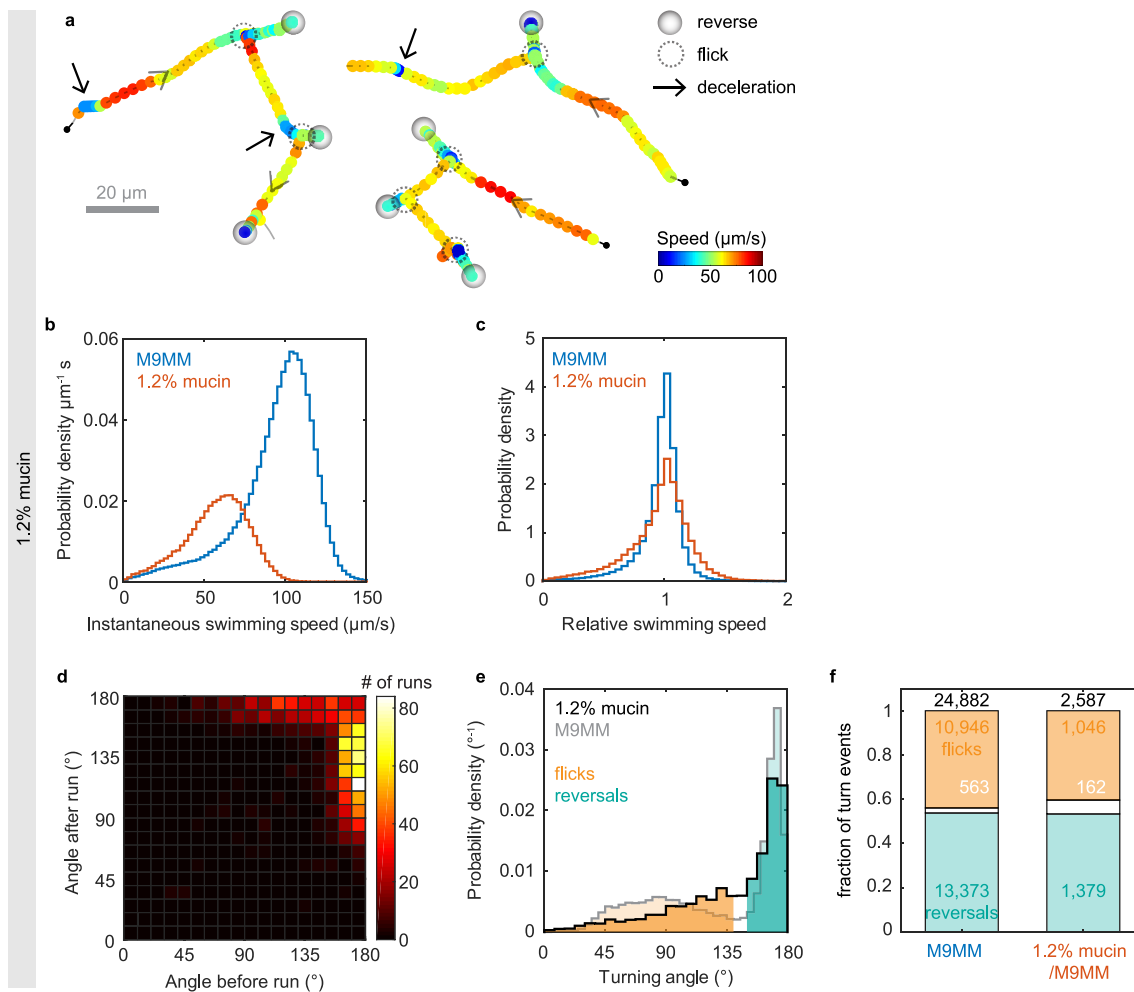


**FIG 5** Run-reverse-flick motility in solutions of 1.2% mucin in M9MM. (a) Three example trajectories in 1.2% mucin, with marked reverse, flick, and deceleration events. (b) Distribution of instantaneous swimming speeds observed in the presence (red) and absence (blue) of mucin. The average speeds are  $57 \mu\text{m/s}$  in mucin and  $94 \mu\text{m/s}$  in M9MM. (c) Distribution of relative swimming speeds in the presence (red) and absence (blue) of mucin. The relative speed is the instantaneous swimming speed divided by the individual's median swimming speed. (d) Bivariate histogram of consecutive turning angles in 1.2% mucin also displays alternating flicks and reversals as well as consecutive reversals, consistent with run-reverse-flick motility. (e) Distribution of turning angles and classification of turn events for trajectories in M9MM (gray; reproduced from Fig. 1d) and in mucin (black). The average flick angle is  $88^\circ \pm 26^\circ$  (mean  $\pm$  SD) in M9MM and  $97^\circ \pm 33^\circ$  in 1.2% mucin/M9MM. The average reversal angle is  $169^\circ \pm 6^\circ$  in M9MM and  $168^\circ \pm 7^\circ$  in mucin. (f) Fraction of turn events classified as flicks (orange), reversals (teal), or unidentified (white) in the absence and presence of 1.2% mucin. Turns of an angle up to  $140^\circ$  are considered flicks, those above  $150^\circ$  are reversals, and those in between  $140^\circ$  and  $150^\circ$  are considered unidentified. Absolute numbers of events for each category are given.

magnitudes before and after a run indicates alternating flicks and reversals, or sequences of reversals, consistent with run-reverse-flick motility (Fig. 5d). The magnitude of the flicks has increased from  $88^\circ \pm 26^\circ$  (mean  $\pm$  standard deviation [SD], 10,946 angles) observed in buffer to  $97^\circ \pm 33^\circ$  (mean  $\pm$  SD, 1,046 angles). As our flick angle measurements combine a reversal and a reorientation occurring in rapid succession, the increased flick angle indicates a decreased reorientation, consistent with increased drag. The fraction of turn events identified as reversals is very similar in the absence and presence of mucin (Fig. 5e). While the fraction of turn events identified as flicks is slightly lower in mucin than in buffer, we attribute this difference to the increased difficulty of identifying flicks due to their increased magnitude. Thus, we conclude that the flick probability is likely very similar in the presence of mucin as in its absence. The observed event rates are compatible with flick probabilities in the range of 88 to 93% in the absence and 81 to 94% in the presence of mucin, depending on whether the unidentified turn events are dominated by flicks or reversals.

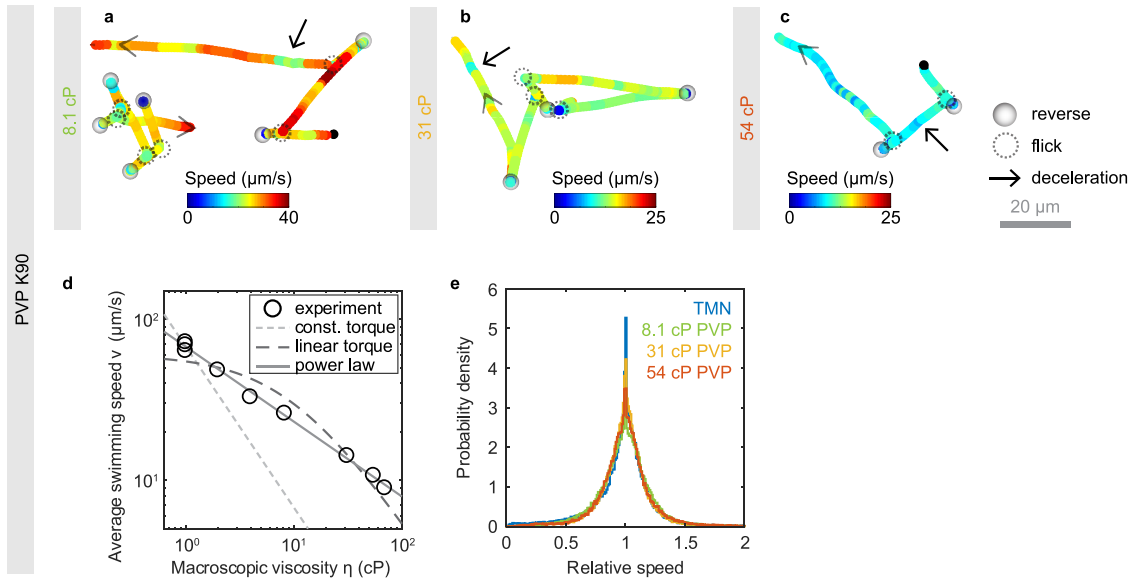


**FIG 6** Run-reverse-flick motility in PVP K90 solutions. (a to c) Example trajectories showing run-reverse-flick motility and variations in swimming speed at concentrations of 2.2%, 4.5%, and 6% PVP K90 in TMN. (d) Average swimming speed as a function of macroscopic PVP K90 viscosity. The dashed and dotted lines represent two different motor torque models under the assumption of Newtonian fluid behavior. The light gray, dotted line indicates a  $\eta^{-1}$  dependence, corresponding to a constant motor torque. The darker dashed line is a fit of the dependence  $v = a/(\eta + b)$  that is expected for a linear torque-speed relationship (40). Parameters  $a = 588 \mu\text{m cP s}^{-1}$  and  $b = 9.7 \text{ cP}$  yield the best error-weighted fit when a fixed relative measurement error in swimming speed is assumed. The gray solid line represents a power law fit with dependence  $\eta^{-0.46}$ . (e) Distribution of relative swimming speeds for different PVP concentrations, reflecting constant variability of swimming speeds. The relative speed is the instantaneous swimming speed divided by the individual's median swimming speed.

The observed turning frequency of 0.49 Hz in mucin matches that observed in buffer. The backward and forward run durations of  $0.17 \pm 0.01 \text{ s}$  (mean  $\pm$  standard errors [SE]) and  $0.71 \pm 0.04 \text{ s}$ , respectively, are also close to the values of  $0.174 \pm 0.002 \text{ s}$  and  $0.62 \pm 0.01 \text{ s}$  observed in buffer. We also still observe temporary decreases in swimming speed during runs (Fig. 5a) but cannot rule out that inhomogeneities in the mucin solution contribute to them. The relative variability in swimming speeds is slightly increased in the presence of mucin, with a coefficient of variation, defined as the ratio of standard deviation and mean, of relative swimming speeds of 0.29 in mucin and 0.25 in buffer (Fig. 5c).

**Run-reverse-flick motility is preserved in dense polymer solutions.** The gut environment likely also contains regions that are denser than the dilute mucin solutions used here. To determine whether *V. cholerae* motility behavior differs qualitatively in denser environments, we observe *V. cholerae* motility in solutions of the synthetic, high-molecular-weight polymer PVP K90 (Fig. 6). Run-reverse-flick motility is still apparent even at macroscopic viscosities more than 50 times that of water where the swimming speed has dropped to  $11 \mu\text{m/s}$  (Fig. 6a to c). With increasing polymer concentration, the associated changes in refractive index cause increasing localization errors. Because these errors can cause ambiguities in trajectory interpretation, we refrain from performing a quantitative turning analysis at this point. Variations in swimming speed during runs are still visually apparent (Fig. 6a to c) and occur at a similar relative amplitude as that in buffer (Fig. 6e).

In a Newtonian liquid with viscosity  $\eta$ , the swimming speed would be expected to decay as  $1/\eta$  if the torque of the flagellar motor remains constant. The average swimming speed of *V. cholerae*, however, decreases more slowly with the macroscopic viscosity of PVP K90 solutions (Fig. 6d). The flagellar motors of *E. coli* (29) and *V. alginolyticus* (30) have been shown to exhibit a complex torque-speed relationship that can be approximated by a constant torque regime at low speeds and high loads and a linear decrease in torque as a function of rotation speed beyond a rotation speed threshold



**TABLE 1** Comparison of motility parameters between strains O395-NT and wild-type O395 in M9MM<sup>a</sup>

Strain	Analyzed trajectory time (s)	Avg swimming speed ( $\mu\text{m/s}$ )	Turning frequency (Hz)	Avg forward run duration (s)	Avg backward run duration (s)
O395-NT	58,029 (23,062)	94	0.49 (28,703)	$0.62 \pm 0.01$ (4,581)	$0.174 \pm 0.002$ (8,180)
O395 (wt)	19,113 (8,017)	88.5	0.47 (8,978)	$0.58 \pm 0.02$ (1,240)	$0.18 \pm 0.01$ (2,283)

<sup>a</sup>Numbers of events on which the value is based are shown in parentheses.

called the knee frequency. A linear torque-speed relationship, in combination with Newtonian hydrodynamics, however, does not provide a good fit to the data (Fig. 6d). In both cases, the measured swimming speeds at high macroscopic viscosity exceed the theoretical expectation. Empirically, a power law fit with an exponent of 0.46 provides a good approximation to the data.

We conclude that run-reverse-flick motility as well as speed variations are present in solutions of both synthetic and natural polymers and, thus, may also occur in the host environment.

**Strain dependence of observations.** While we performed our experiments with strain O395-NT (21), a mutant of classical strain O395 that carries a deletion of both subunits of the cholera toxin (ctxAB), visual inspection of trajectories obtained for wild-type O395 reveals no differences in behavior (Fig. S3). Both run-reverse-flick motility and speed modulation during runs are present in both strains. Automated trajectory analysis reveals similar turning frequencies as well as very similar average backward and forward run durations for strains O395-NT and wild-type O395 (Table 1). The observed turning frequency of 0.49 Hz aligns well with the value of approximately 0.6 Hz previously reported (31) for O395-N1 ( $\Delta\text{ctxA}$  in O395 [21]) but is much higher than the value of 0.14 Hz previously reported for the El Tor strain C6709-1 (13). Together with the finding that smooth-swimming mutants possess greater infectivity (13), this discrepancy raises the intriguing question whether selection on turning frequency may have contributed to the displacement of classical strains by El Tor strains in the current *V. cholerae* pandemic.

## DISCUSSION

During its life cycle, *V. cholerae* encounters a wide range of different environments. Outside the host, it is found in freshwater and in brackish waters both as individual, planktonic swimmers and as biofilms that grow, for instance, on the surface of phytoplankton, zooplankton, and other chitinous particles (32). Inside the host, the bacterium encounters the complex 3D environments of the digestive system with a wide range of viscosities, porosities, and inhomogeneities. While our observations for *V. cholerae* swimming in buffer likely translate to planktonic cells in natural aquatic environments such as brackish waters, the host environment is not characterized well enough to determine with certainty how well the polymer solutions used in our experiments approximate it. *V. cholerae* colonizes the small intestine, which is lined by a loose, nonattached mucus layer (33, 34). For the colon, which additionally possesses a thick attached mucus layer with an estimated mucin concentration of approximately 6% (35), the concentration of the nonattached, loose layer has been estimated to be approximately four times lower than that of the attached layer (36), likely similar to the mucin concentration of 1.2% used in our experiments. Thus, we expect that our mucin solutions approximate the concentration of the loose mucus layer of the small intestine, although properties of the salivary mucin MUC5B used here may differ from those of intestinal mucins. While detailed rheological data for the MUC5B concentrations used here are not available, literature values on other mucins and more dilute MUC5B solutions suggest a macroscopic viscosity in the range of 2 to 15 cP (see Note S2 in the supplemental material).

In contrast to our finding of a very similar turning frequency and flick probability in buffer and in 1.2% purified salivary mucin solutions, a recent study (19) reports a decreased turning frequency and decreased flick probability for *V. cholerae* in solutions

of 2% porcine gastric mucin, prepared from commercially available, rehydrated dried porcine gastric mucin. Given *V. cholerae*'s chemotactic attraction to mucus (37), the reported decrease in turning frequency might reflect a transient chemotactic response to the mucin solution. Our experimental approach limits such transient effects by incubating the bacteria in the motility medium with or without mucin for more than 30 min to allow for adaptation to the new environment. In addition, reports that rehydrated dried mucus does not recapitulate characteristic rheological properties of purified mucus (38) suggest that the properties of rehydrated and purified mucin solutions are not comparable (39). The flick probability is expected to depend on the torque exerted by the flagellar motor and, thus, drops with decreasing sodium-motive force, which coincides with a drop in speed (18) (Fig. 2). While at increasing viscosity the swimming speed also decreases, the motor torque is expected to remain constant or increase (30). Therefore, a decreased flick probability is physically not expected at higher viscosity. The recently reported drop in flick probability in mucin (19) might result from the increased difficulty in disambiguating flicks from reversals because of the larger flick angles in mucin.

Work on *E. coli* swimming in PVP K90 solutions indicates that, due to strong shear thinning, the resulting bacterial motility behavior depends only on macroscopic viscosities, not detailed rheological properties, with the cell body experiencing the solution viscosity and the flagellum the solvent viscosity (40) (Note S2). Shear thinning or other non-Newtonian effects may contribute to the slow decrease in swimming speed with macroscopic viscosity we observe in PVP solutions. Additional contributions may arise, however, from the ability of the flagellar motor to remodel itself by increasing the number of torque-generating stators in response to load increases such that different loads result in different torque-speed curves (41, 42). Mucus and mucin also exhibit strong shear thinning (39, 43). The relative decrease in swimming speed we observe in our mucin solutions is similar to that observed in PVP solutions, with a macroscopic viscosity of approximately 3 cP (Fig. 6d and Note S2). The range of PVP viscosities we cover aligns with the 1- to 30-cP range of macroscopic viscosities determined for mucus from the small intestine (44). Elastic effects are not expected to play a role for either PVP or mucin at the concentrations studied here (40, 45). More generally, our finding that the motility behavior is qualitatively similar in solutions of the natural glycoprotein polymer mucin and over a range of concentrations of the synthetic polymer PVP suggest that our observations translate to a broader range of polymer solutions.

The swimming speed variations we observe might be related to pauses in swimming that have been reported in *Pseudomonas putida* (46), *Pseudomonas aeruginosa* (47), and *Azospirillum brasilense* (48) or to the pauses in flagellar rotation that have been reported in *E. coli* (49), *Rhodobacter sphaeroides* (50), and *P. aeruginosa* (51). For *E. coli*, a correlation between the turning and flagellar pausing frequencies was observed both between mutant strains and between individuals of the same strain (52). We detect no correlation between individual turning and deceleration frequency for *V. cholerae* (Fig. S4f), but the typically small number of events per trajectory in our data is insufficient to rule out a correlation. We also cannot confidently determine whether deceleration events appear only in forward runs or in both run directions, as most backward runs are too short to assign a reliable baseline speed against which variations can be detected. We note that, during the events we observe, swimming never appears to stop but only decreases in speed, indicating that the flagellum continues to rotate but at a lower speed. In *E. coli*, the speed of flagellar rotation is varied in response to the load on the flagellar motor by changes in the number of torque-producing stators that drive motor rotation (41, 42). Active modulation of flagellar rotation speeds by the chemotaxis signaling system has been reported for proton-driven, unidirectional, peritrichous flagella in *V. alginolyticus* (53), which conditionally expresses these lateral flagella in addition to its polar flagellum, as well as in *Rhizobium meliloti* (54). Transient changes in swimming speed in response to changes in oxygen

availability have been reported for *A. brasilense* (55), whose motility is driven by a single, polar, bidirectional flagellum. Tethering experiments may be able to more closely determine the nature and determinants of the modulation in flagellar rotation speed that underlie the swimming speed variation we observe in *V. cholerae*.

*V. cholerae*'s asymmetry in run durations increases its ability to spread randomly (Fig. 3e). In addition, backward swimming segments typically display more trajectory curvature in the vicinity of surfaces than forward swimming segments (22, 56, 57) (Fig. S2). Thus, a bias for forward swimming may further increase dispersal in the vicinity of surfaces compared to a symmetric scenario. While the potential adaptive value of the asymmetric run duration scheme has yet to be evaluated, one possibility is that strong random dispersal is selected for at some point in the *V. cholerae* life cycle. Interestingly, previous work has consistently found that smooth-swimming mutants that suppress turning outcompete the wild type during infection (4, 13, 37, 58). Such mutants are also expected to display a strongly enhanced effective diffusion coefficient. Another possibility is that asymmetric run durations have a favorable effect on chemotactic ability, although Altindal et al. (27) have argued that symmetric run durations maximize the chemotactic drift velocity in *V. alginolyticus*. While it may seem surprising that two *Vibrio* species performing run-reverse-flick motility pursue different strategies in relative run durations, we note that they also differ in other aspects of their motility behavior. In contrast to *V. cholerae*, *V. alginolyticus* responds to viscous environments by expressing lateral flagella in addition to its polar flagellum (59). These differences suggest either different selective pressures or different adaptive strategies in motility behaviors between the two species.

Run-reverse-flick motility with very short backward swimming segments has also been observed in *Shewanella putrefaciens* (60) and bears some similarities to *E. coli*'s run-tumble motility, where CW rotation does not produce locomotion but reorientation. These two mechanisms, however, differ in how the degree of reorientation can be controlled. In the run-tumble-like scenario, the magnitude of the reorientation can be increased by prolonging backward run segments, or CW rotation intervals, akin to the relationship between tumble duration and tumble angle that has been observed in *E. coli* (61). In run-reverse-flick motility, in contrast, the magnitude of flick angles is fixed for each individual by the hydrodynamic drag acting on it (20) and, thus, is expected to be independent of the duration of CW rotation intervals. The average amount of reorientation, however, also depends on the flicking probability determined by the flagellar motor torque, which can vary with environmental conditions such as salinity (Fig. 2) or nutrient concentrations (62). These differences are likely to affect both random motility and chemotaxis. For instance, the chemotactic precision of the run-reverse-flick bacterium *V. alginolyticus* has been shown to be enhanced by the chemoattractant-dependent modulation of the flicking probability (62) via the swimming speed.

Future work should address *V. cholerae*'s chemotactic mechanism. The well-studied chemotactic strategy of *E. coli* consists of extending average CCW rotation intervals and shortening average CW rotation intervals in response to favorable chemotactic sensory input, extending runs up the gradient. The CW bias, that is, the fraction of time spent on CW rotation, thereby serves as a convenient proxy for the turning frequency, which guides chemotaxis. Other species displaying run-reverse-flick motility, *V. alginolyticus* (63) and *C. crescentus* (22), as well as the run-reverse swimmer *P. aeruginosa* (47), instead respond to favorable signals by extending the current flagellar rotation interval regardless of direction and perform chemotaxis by modulating the turning frequency without substantial change in the bias. While *V. cholerae*'s swimming pattern is closer to the latter category, its short CW rotation intervals are reminiscent of *E. coli*'s short tumbles.

Butler and Camilli (13) termed smooth-swimming chemotaxis mutants CCW-biased and frequently turning mutants CW-biased, based on the well-characterized motility phenotypes of the homologous mutants in *E. coli*, and attributed their differences in

**TABLE 2** Composition of growth and motility media

Medium	Composition
LB5	1% Bacto tryptone, 0.5% Bacto yeast extract, 0.5% NaCl, pH 7.0
LB10	1% Bacto tryptone, 0.5% Bacto yeast extract, 1% NaCl, pH 7.0
TG	1% Bacto tryptone, 0.5% NaCl, 0.5% (wt/vol) glycerol, pH 7.1
M9GM	M9 salts (from 5 × stock; 47.7 mM Na <sub>2</sub> HPO <sub>4</sub> , 22 mM KH <sub>2</sub> PO <sub>4</sub> , 8.55 mM NaCl, 9.35 mM NH <sub>4</sub> Cl) (Sigma), 77 mM NaCl, 0.4% pyruvate, 2 mM MgSO <sub>4</sub> , 1 mM CaCl <sub>2</sub> , pH 7.0
M9MM	M9 salts (from 5 × stock; 47.7 mM Na <sub>2</sub> HPO <sub>4</sub> , 22 mM KH <sub>2</sub> PO <sub>4</sub> , 8.55 mM NaCl, 9.35 mM NH <sub>4</sub> Cl) (Sigma), 77 mM NaCl, 5 mM glucose, 2 mM MgSO <sub>4</sub> , 1 mM CaCl <sub>2</sub> , pH 7.0
NoNa-M9MM	47.7 mM K <sub>2</sub> HPO <sub>4</sub> , 22 mM KH <sub>2</sub> PO <sub>4</sub> , 8.55 mM KCl, 9.35 mM NH <sub>4</sub> Cl, 5 mM glucose, 2 mM MgSO <sub>4</sub> , 1 mM CaCl <sub>2</sub> , pH 7.0
TMN	50 mM Tris-HCl, 300 mM NaCl, 5 mM MgCl <sub>2</sub> , 5 mM glucose, pH 7.5
PYE	0.2% Bacto peptone, 0.1% Bacto yeast extract, 1 mM MgSO <sub>4</sub> , 0.5 mM CaCl <sub>2</sub> , pH 7.0

infectivity to the bias in flagellar rotation direction. The bias was, however, not explicitly characterized. Given that bias and turning frequency have been shown to be decoupled in other run-reverse-flick-performing bacteria and that bias and turning frequency are expected to have distinct effects on motility and chemotaxis (26), future work should address which of these factors drives the observed differences in infectivity. Insights might be gained, in particular, from infectivity assays on smooth-swimming, CW-rotating mutants. We envision that quantitative characterization of motility behaviors of mutants with infectivity phenotypes may present a key tool toward a mechanistic understanding of how motility and chemotaxis behaviors contribute to *V. cholerae* pathogenicity.

## MATERIALS AND METHODS

**Bacterial culturing.** Overnight cultures were inoculated from individual *V. cholerae* (O395-NT [21] or O395) colonies, grown on 1.5% agar LB5 plates streaked from glycerol stock, and grown to saturation in 2 ml LB5 (Table 2 lists compositions of media) at 30°C and 250 rpm. All media were complemented with 100 μg/ml kanamycin for the O395-NT strain. Day cultures were inoculated at a dilution of 1:200 (vol/vol) in M9 minimal medium with pyruvate (M9GM) and grown at 30°C to an optical density (OD) between 0.350 and 0.400 at 600 nm, unless specified otherwise. While LB5 and TG were previously used in *V. cholerae* motility studies (5, 13, 23, 31, 64–66), M9GM yielded higher swimming speeds and lower nonmotile fractions, similar to another recent study (67). We found that an OD range of 0.35 to 0.4 yielded average swimming speeds above 90 μm/s and a typical motile fraction above 85%.

**Sample preparation.** Sample chambers with a height of approximately 300 μm were created by using two strips consisting of 3 layers of Parafilm as spacers between a microscopy slide and a no. 1 coverslip. The chamber was then heated on a hot plate and pressed to seal. For samples with mucin, only 2 layers of Parafilm were used to reduce sample volumes. Cells were diluted by 1:100 in M9MM (or fresh growth medium during protocol optimization tests displayed in Fig. 1a and c), incubated at room temperature for 45 min, unless specified otherwise, to allow adaptation to the motility medium, and then flowed into the chamber. Cell solutions are only pipetted with cut pipet tips to avoid shear damage to the flagella. For samples with polymer solutions, cells were first pelleted by centrifugation at 2,000 relative centrifugal force (rcf) for 8 min, resuspended in the relevant motility medium, diluted 1:200 in the polymer solution, incubated at room temperature for 40 to 60 min, and flowed into the chamber. The ends of the filled chamber were then sealed with molten valap (a mixture of vaseline, lanolin, and paraffin) and immediately brought to the microscope for data acquisition. For motility in M9MM, three to five such samples were prepared and inspected within a period of 10 min for each of three biological replicates for strain O395-NT and one for wild-type O395. For PVP polymer solution experiment, one sample was prepared and inspected per concentration studied, all within a period of 30 min. For growth condition tests and mucin solution experiment, two to three samples were prepared and inspected for one biological replicate.

**Data acquisition.** Phase contrast microscopy recordings were obtained at room temperature (~22°C) on a Nikon Ti-E inverted microscope using an sCMOS camera (PCO Edge 4.2; pixel size, 6.5 μm) and a 40× lens objective (Nikon CFI SPlan Fluor ELWD 40× ADM Ph2; correction collar set to 1.2 mm to induce spherical aberrations [20]) focused approximately 130 μm above the chamber's internal bottom surface. The illumination was adjusted to yield approximately 20,000 counts per pixel. Recordings were saved as 16-bit tiff files. For each sample in M9MM, one recording with a duration of 2 to 2.2 min and a frame rate of 30 fps was obtained immediately after placing the sample on the microscope. The three replicate experiments for O395-NT generated a cumulative 23 min of video recordings. For each PVP sample, one recording was obtained at 30 fps or 15 fps for concentrations above or under 3%, respectively. During the same experiment, one control acquisition in TMN at 30 fps was done before, in the middle of, and after acquisitions in PVP. For mucin samples, two 1.7-min recordings were obtained at 15 fps. For growth medium tests, two to three recordings of 1 to 3 min were obtained at 30 fps. Numbers

of biological and technical replicates as well as duration of acquisitions are summarized in Table S1 in the supplemental material.

**Data analysis.** Video recordings were binned by a factor of  $2 \times 2$  by averaging counts and then subjected to a background correction procedure based on dividing the image by a pixel-wise median computed across a sliding window of 101 frames, except for data acquired for mucin experiments, where a sliding window of 41 frames was used. 3D trajectories were extracted from phase contrast recordings using a high-throughput 3D tracking method based on image similarity between bacteria and a reference library (20). 3D bacterial trajectories were extracted in a tracking volume of approximately  $350 \mu\text{m}$  by  $300 \mu\text{m}$  laterally ( $x, y$ ) and  $200 \mu\text{m}$  in depth ( $z$ ) for typically several dozen individuals at a time. Positions were smoothed using 2nd order ADMM-based trend filtering (68) with regularization parameter  $\lambda = 0.3$  unless stated otherwise (Table S1), and three-dimensional velocities were computed as forward differences in positions divided by the time interval between frames. All trajectories with an average speed below a  $20\text{-}\mu\text{m/s}$  threshold, unless stated otherwise, were deemed nonmotile and discarded. For PVP polymer solutions, the nonmotile threshold was adjusted to the population's swimming speed (Table S1). For samples with 1.3 and 7.4 mM  $\text{Na}^+$ , we used  $\lambda = 0.8$  and a nonmotile threshold of  $10 \mu\text{m/s}$ .

**Run-reverse-flick analysis.** The bacteria's motility behavior in M9MM was analyzed based on trajectories with a duration of at least 1 s, totaling 23,062 trajectories (58,029 s) and 8,017 trajectories (19,113 s) for strain O395-NT and O395, respectively. The turning event detection is based on the local rate of angular change, computed from the dot product between the sums of the two consecutive velocity vectors preceding and subsequent to a time point. The threshold for a turn to begin is an  $\alpha$ -fold rate relative to the median rate of angular change during the trajectory's run segments, as determined in three iterations of the procedure. We determined by visual inspection of trajectories that a factor of  $\alpha = 8$  gave satisfactory results. A turn ends when the local rate of angular change is below the threshold again. The 3D turning angle for a turn beginning at frame  $i$  and ending at point  $j$  is computed as the angle between the sum of the instantaneous velocity vectors at frames  $i-2$  and  $i-1$  and the sum of those at frames  $j$  and  $j + 1$ . Turning events were labeled flicks or reversals if the turning angle was below  $140^\circ$  or above  $150^\circ$ , respectively. The bacterial orientation during runs (forward/backward) was assigned based on the identity of the two bordering turning events. Backward and forward runs were identified as runs with a flick at the end or at the beginning of the run and a reversal at the other end of the run. For the motility analysis of the O395-NT strain, a total of 8,180 backward and 4,581 forward runs were identified out of 18,533 runs, within a subpopulation of 5,932 trajectories (20,299-s cumulative duration). For the motility analysis of the wild-type O395 strain, 2,283 backward and 1,240 forward runs were identified out of 5,425 runs within a subpopulation of 1,765 trajectories with a cumulative duration of 5,816 s. For experiments on O395-NT in sodium concentrations of 136 mM, 7.4 mM, and 1.8 mM, displayed in Fig. 2, we detected 2,769, 6,093, and 10,035 turning events with measurable turning angles in 2,683, 5,089, and 4,083 trajectories, respectively. For O395 in mucin solutions, we obtained and analyzed 2,327 trajectories with a total duration of 6,027 s, containing 2,587 turning events with measurable turning angle, enabling us to identify 707 backward and 385 forward runs.

**Deceleration analysis.** Runs with a duration of more than 0.33 s and an average speed above  $30 \mu\text{m/s}$  were screened for segments of decreased speed, here called "decelerations." A deceleration begins when the instantaneous speed drops below a threshold for two consecutive frames and ends when the speed is above the threshold again for two consecutive frames. The threshold is defined as a fraction  $\beta$  of the run's median speed outside deceleration events, as determined iteratively in two rounds of the detection procedure. We tested a range of  $\beta = 0.3$  to 0.9 (Fig. S4). Figure 4 shows results obtained for  $\beta = 0.75$ .

**Polymer solutions.** O395-NT was tracked in solutions of the linear polymer polyvinylpyrrolidone (average molecular weight of about 360,000 kDa; PVP K90; Sigma 81440) with concentrations of ranging from 0.9 to 6.7% (wt/wt) in TMN, or of human MUC5B mucin purified from human saliva (69) (a kind gift of K. Ribbeck) at 1.2% (wt/wt) in M9MM. A volume of 3.3 mg lyophilized mucin was dissolved in  $275 \mu\text{l}$  M9MM by shaking at 250 rpm at  $4^\circ\text{C}$  for 5 h. Two hours before the experiment, the solution was slowly pipetted to further homogenize it and shaken at room temperature at 300 rpm. Macroscopic viscosity measurements for PVP K90 solutions with concentrations in the 0% to 7.2% range were obtained using two falling-ball viscometers (2- to 20-cP range and 10- to 100-cP range; Gilmont) at room temperature ( $21^\circ\text{C}$ ) after calibration using viscosity standards of 11.6 and 48.0 cP (general purpose standards D10 and N26, respectively; Paragon Scientific). The relationship between PVP concentration and viscosity was extracted as a second-order polynomial fit with a forced intercept of 0.98 cP at 0% PVP (Fig. S5).

**Low-sodium motility experiment.** We varied the motility medium's  $\text{Na}^+$  concentration at constant ionic strength by mixing M9MM with a buffer identical to M9MM, except that all sodium-containing ingredients were replaced by the equivalent potassium-containing ones. NaCl was replaced by KCl, and  $\text{Na}_2\text{HPO}_4$  was replaced by  $\text{K}_2\text{HPO}_4$  (NoNa-M9MM) (Table 2). The experiments were performed as described for experiments with M9MM, except that the culture was not diluted into the motility medium but pelleted at 2,000 rcf for 8 min before gentle resuspension in the appropriate motility medium to precisely control the final  $\text{Na}^+$  concentration.

**C. crescentus experiment.** *C. crescentus* has a dimorphic life cycle: a stalked cell attached to a surface divides and releases a motile daughter cell. We obtained motile cells by a modified plate-release protocol (70). An overnight culture inoculated from an individual *C. crescentus* (CB15, ATCC 19089) colony, grown on 1.5% agar PYE plates streaked from frozen glycerol stock stored at  $-80^\circ\text{C}$ , was grown to saturation in 2 ml PYE at  $30^\circ\text{C}$  and 200 rpm. The overnight culture was diluted 1:100 in fresh PYE and then grown in volumes of 0.5 ml in a 24-well plate incubated at  $30^\circ\text{C}$  without agitation for 24 h. The wells were washed and refilled with fresh PYE and placed at room temperature on a shaker at 130 rpm

for another 24 h. At that stage, the bottoms of the wells were covered with a dense carpet of stalked cells continuously producing motile cells. For experiments, a well was rinsed three times with PYE, and then 0.5 ml of fresh PYE was placed in the well and removed after 5 min, containing the newly separated motile cells. Such cell suspensions were immediately injected into a sample chamber and placed on the microscope. Recordings with a duration of 1.5 min were obtained as described for *V. cholerae*. Data analysis was performed as described for *V. cholerae*, except a threshold factor  $\alpha = 6$  was used for turn event detection, as it seemed to produce more accurate results based on visual inspection.

**Data availability.** All trajectory data as well as our Matlab turn event detection code are available in the Harvard Dataverse repository at <https://doi.org/10.7910/DVN/FNWZ2Q> (71).

## SUPPLEMENTAL MATERIAL

Supplemental material is available online only.

**SUPPLEMENTAL FILE 1**, PDF file, 1.1 MB.

## ACKNOWLEDGMENTS

Purified mucin was a kind gift from Katharina Ribbeck (MIT). *V. cholerae* strains O395 and O395-NT were a kind gift from Edward Ryan (MGH/Harvard Medical School). We thank Chloe M. Wu for advice on mucin experiments. This research was supported by the Rowland Institute as well as the Rowland Institute Postdoctoral Fellow and Undergraduate Program, funded by the Rowland Foundation.

K.M.T. and M.G. conceived the research. M.M., A.M., and M.G. performed growth condition tests. A.M. and M.G. performed all other experiments on *V. cholerae*. M.G. performed experiments on *C. crescentus* as well as viscosity measurements. M.G. developed the turning event analysis. A.M. and M.G. contributed to performing and evaluating turning event analysis. A.M. noticed deceleration events, and M.G. developed and performed deceleration event analysis. M.G. and K.M.T. wrote the manuscript. All authors commented on the manuscript.

## REFERENCES

- Almagro-Moreno S, Pruss K, Taylor RK. 2015. Intestinal colonization dynamics of *Vibrio cholerae*. *PLoS Pathog* 11:e1004787-11. <https://doi.org/10.1371/journal.ppat.1004787>.
- Butler SM, Camilli A. 2005. Going against the grain: chemotaxis and infection in *Vibrio cholerae*. *Nat Rev Microbiol* 3:611–620. <https://doi.org/10.1038/nrmicro1207>.
- Butler SM, Nelson EJ, Chowdhury N, Faruque SM, Calderwood SB, Camilli A. 2006. Cholera stool bacteria repress chemotaxis to increase infectivity. *Mol Microbiol* 60:417–426. <https://doi.org/10.1111/j.1365-2958.2006.05096.x>.
- Lee SH, Butler SM, Camilli A. 2001. Selection for in vivo regulators of bacterial virulence. *Proc Natl Acad Sci U S A* 98:6889–6894. <https://doi.org/10.1073/pnas.111581598>.
- Silva AJ, Leitch GJ, Camilli A, Benitez JA. 2006. Contribution of hemagglutinin/protease and motility to the pathogenesis of El Tor biotype cholera. *Infect Immun* 74:2072–2079. <https://doi.org/10.1128/IAI.74.4.2072-2079.2006>.
- Liu Z, Miyashiro T, Tsou A, Hsiao A, Goulian M, Zhu J. 2008. Mucosal penetration primes *Vibrio cholerae* for host colonization by repressing quorum sensing. *Proc Natl Acad Sci U S A* 105:9769–9774. <https://doi.org/10.1073/pnas.0802241105>.
- Rui H, Ritchie JM, Bronson RT, Mekalanos JJ, Zhang Y, Waldor MK. 2010. Reactogenicity of live-attenuated *Vibrio cholerae* vaccines is dependent on flagellins. *Proc Natl Acad Sci U S A* 107:4359–4364. <https://doi.org/10.1073/pnas.0915164107>.
- Wang Z, Lazinski DW, Camilli A. 2016. Immunity provided by an outer membrane vesicle cholera vaccine is due to O-antigen-specific antibodies inhibiting bacterial motility. *Infect Immun* 85:209–209. <https://doi.org/10.1128/IAI.00626-16>.
- Millet YA, Alvarez D, Ringgaard S, von Andrian UH, Davis BM, Waldor MK. 2014. Insights into *Vibrio cholerae* intestinal colonization from monitoring fluorescently labeled bacteria. *PLoS Pathog* 10:e1004405-14. <https://doi.org/10.1371/journal.ppat.1004405>.
- Benenson AS, Islam MR, Greenough WB. 1964. Rapid identification of *Vibrio cholerae* by darkfield microscopy. *Bull World Health Organ* 30:827–831.
- Weil AA, LaRocque RC. 2020. Cholera and other vibrios, 10th ed. Elsevier Inc, New York, NY. <https://doi.org/10.1016/B978-0-323-55512-8.00047-8>.
- Chowdhury F, Khan AI, Faruque ASG, Ryan ET. 2010. Severe, acute watery diarrhea in an adult. *PLoS Negl Trop Dis* 4:e898. <https://doi.org/10.1371/journal.pntd.0000898>.
- Butler SM, Camilli A. 2004. Both chemotaxis and net motility greatly influence the infectivity of *Vibrio cholerae*. *Proc Natl Acad Sci U S A* 101:5018–5023. <https://doi.org/10.1073/pnas.0308052101>.
- Ringgaard S, Schirner K, Davis BM, Waldor MK. 2011. A family of ParA-like ATPases promotes cell pole maturation by facilitating polar localization of chemotaxis proteins. *Genes Dev* 25:1544–1555. <https://doi.org/10.1101/gad.2061811>.
- Ortega DR, Kjaer A, Briegel A. 2020. The chemosensory systems of *Vibrio cholerae*. *Mol Microbiol* 114:367–376. <https://doi.org/10.1111/mmi.14520>.
- Ringgaard S, Yang W, Alvarado A, Schirner K, Briegel A, DiRita VJ. 2018. Chemotaxis arrays in *Vibrio* species and their intracellular positioning by the ParC/ParP system. *J Bacteriol* 200:e00793-17. <https://doi.org/10.1128/JB.00793-17>.
- Xie L, Altindal T, Chattopadhyay S, Wu X-L. 2011. Bacterial flagellum as a propeller and as a rudder for efficient chemotaxis. *Proc Natl Acad Sci U S A* 108:2246–2251. <https://doi.org/10.1073/pnas.1011953108>.
- Son K, Guasto JS, Stocker R. 2013. Bacteria can exploit a flagellar buckling instability to change direction. *Nature Phys* 9:494–498. <https://doi.org/10.1038/nphys2676>.
- Frederick A, Huang Y, Pu M, Rowe-Magnus DA. 2020. *Vibrio cholerae* type VI activity alters motility behavior in mucin. *J Bacteriol* 202:e00261-20. <https://doi.org/10.1128/JB.00261-20>.
- Taute KM, Gude S, Tans SJ, Shimizu TS. 2015. High-throughput 3D tracking of bacteria on a standard phase contrast microscope. *Nat Commun* 6:8776–8779. <https://doi.org/10.1038/ncomms9776>.
- Mekalanos JJ, Swartz DJ, Pearson GDN, Harford N, Groyne F, de Wilde M. 1983. Cholera toxin genes: nucleotide sequence, deletion analysis and vaccine development. *Nature* 306:551–557. <https://doi.org/10.1038/306551a0>.
- Grognot M, Taute KM. 2021. A multiscale 3D chemotaxis assay reveals bacterial navigation mechanisms. *Commun Biol* 4:669. <https://doi.org/10.1038/s42003-021-02190-2>.

23. Kojima S, Yamamoto K, Kawagishi I, Homma M. 1999. The polar flagellar motor of *Vibrio cholerae* is driven by an Na<sup>+</sup> motive force. *J Bacteriol* 181:1927–1930. <https://doi.org/10.1128/JB.181.6.1927-1930.1999>.
24. Lauga E, DiLuzio WR, Whitesides GM, Stone H. 2006. Swimming in circles: motion of bacteria near solid boundaries. *Biophys J* 90:400–412. <https://doi.org/10.1529/biophysj.105.069401>.
25. Morse M, Bell J, Li G, Tang JX. 2015. Flagellar motor switching in *Caulobacter crescentus* obeys first passage time statistics. *Phys Rev Lett* 115:312. <https://doi.org/10.1103/PhysRevLett.115.198103>.
26. Taktikos J, Stark H, Zaburdaev V. 2013. How the motility pattern of bacteria affects their dispersal and chemotaxis. *PLoS One* 8:e81936-16. <https://doi.org/10.1371/journal.pone.0081936>.
27. Altindal T, Xie L, Wu X-L. 2011. Implications of three-step swimming patterns in bacterial chemotaxis. *Biophys J* 100:32–41. <https://doi.org/10.1016/j.bpj.2010.11.029>.
28. Bansil R, Turner BS. 2018. The biology of mucus: composition, synthesis and organization. *Adv Drug Deliv Rev* 124:3–15. <https://doi.org/10.1016/j.addr.2017.09.023>.
29. Chen X, Berg HC. 2000. Torque-speed relationship of the flagellar rotary motor of *Escherichia coli*. *Biophys J* 78:1036–1041. [https://doi.org/10.1016/S0006-3495\(00\)76662-8](https://doi.org/10.1016/S0006-3495(00)76662-8).
30. Sowa Y, Hotta H, Homma M, Ishijima A. 2003. Torque-speed relationship of the Na<sup>+</sup>-driven flagellar motor of *Vibrio alginolyticus*. *J Mol Biol* 327:1043–1051. [https://doi.org/10.1016/s0022-2836\(03\)00176-1](https://doi.org/10.1016/s0022-2836(03)00176-1).
31. Hyakutake A, Homma M, Austin MJ, Boin MA, Häse CC, Kawagishi I. 2005. Only one of the five CheY homologs in *Vibrio cholerae* directly switches flagellar rotation. *J Bacteriol* 187:8403–8410. <https://doi.org/10.1128/JB.187.24.8403-8410.2005>.
32. Teschler JK, Zamorano-Sánchez D, Utada AS, Warner CJA, Wong GCL, Linington RG, Yildiz FH. 2015. Living in the matrix: assembly and control of *Vibrio cholerae* biofilms. *Nat Rev Microbiol* 13:255–268. <https://doi.org/10.1038/nrmicro3433>.
33. Atuma C, Strugala V, Allen A, Holm L. 2001. The adherent gastrointestinal mucus gel layer: thickness and physical state in vivo. *Am J Physiol Gastrointest Liver Physiol* 280:G922–G929. <https://doi.org/10.1152/ajpgi.2001.280.5.G922>.
34. Johansson MEV, Sjövall H, Hansson GC. 2013. The gastrointestinal mucus system in health and disease. *Nat Rev Gastroenterol Hepatol* 10:352–361. <https://doi.org/10.1038/nrgastro.2013.35>.
35. Podolsky DK, Isselbacher KJ. 1983. Composition of human colonic mucin. Selective alteration in inflammatory bowel disease. *J Clin Invest* 72:142–153. <https://doi.org/10.1172/jci110952>.
36. Johansson MEV, Phillipson M, Petersson J, Velcich A, Holm L, Hansson GC. 2008. The inner of the two Muc2 mucin-dependent mucus layers in colon is devoid of bacteria. *Proc Natl Acad Sci U S A* 105:15064–15069. <https://doi.org/10.1073/pnas.0803124105>.
37. Freter R, O'Brien PC. 1981. Role of chemotaxis in the association of motile bacteria with intestinal mucosa: chemotactic responses of *Vibrio cholerae* and description of motile nonchemotactic mutants. *Infect Immun* 34:215–221. <https://doi.org/10.1128/iai.34.1.215-221.1981>.
38. Kočevár-Nared J, Kristl J, Šmid-Korbar J. 1997. Comparative rheological investigation of crude gastric mucin and natural gastric mucin. *Biomaterials* 18:677–681. [https://doi.org/10.1016/s0142-9612\(96\)00180-9](https://doi.org/10.1016/s0142-9612(96)00180-9).
39. Celli JP, Turner BS, Afdhal NH, Ewoldt RH, McKinley GH, Bansil R, Erramilli S. 2007. Rheology of gastric mucin exhibits a pH-dependent Sol–Gel transition. *Biomacromolecules* 8:1580–1586. <https://doi.org/10.1021/bm0609691>.
40. Martínez V, Schwarz-Linek J, Reufer M, Wilson LG, Morozov AN, Poon WCK. 2014. Flagellated bacterial motility in polymer solutions. *Proc Natl Acad Sci U S A* 111:17771–17776. <https://doi.org/10.1073/pnas.1415460111>.
41. Lele PP, Hosu BG, Berg HC. 2013. Dynamics of mechanosensing in the bacterial flagellar motor. *Proc Natl Acad Sci U S A* 110:11839–11844. <https://doi.org/10.1073/pnas.1305885110>.
42. Tipping MJ, Delalez NJ, Lim R, Berry RM, Armitage JP. 2013. Load-dependent assembly of the bacterial flagellar motor. *mBio* 4:e00551-13. <https://doi.org/10.1128/mBio.00551-13>.
43. Lai SK, Wang Y-Y, Wirtz D, Hanes J. 2009. Micro- and macrorheology of mucus. *Adv Drug Deliv Rev* 61:86–100. <https://doi.org/10.1016/j.addr.2008.09.012>.
44. Macierzanka A, Mackie AR, Krupa L. 2019. Permeability of the small intestinal mucus for physiologically relevant studies: impact of mucus location and ex vivo treatment. *Sci Rep* 9:17516. <https://doi.org/10.1038/s41598-019-53933-5>.
45. Georgiades P, Pudney PDA, Thornton DJ, Waigh TA. 2014. Particle tracking microrheology of purified gastrointestinal mucins. *Biopolymers* 101:366–377. <https://doi.org/10.1002/bip.22372>.
46. Theves M, Taktikos J, Zaburdaev V, Stark H, Beta C. 2013. A bacterial swimmer with two alternating speeds of propagation. *Biophys J* 105:1915–1924. <https://doi.org/10.1016/j.bpj.2013.08.047>.
47. Cai Q, Li Z, Ouyang Q, Luo C, Gordon VD. 2016. Singly flagellated *Pseudomonas aeruginosa* chemotaxes efficiently by unbiased motor regulation. *mBio* 7:e00013-16. <https://doi.org/10.1128/mBio.00013-16>.
48. Mukherjee T, Elmas M, Vo L, Alexiades V, Hong T, Alexandre G. 2019. Multiple CheY homologs control swimming reversals and transient pauses in *Azospirillum brasilense*. *Biophys J* 116:1527–1537. <https://doi.org/10.1016/j.bpj.2019.03.006>.
49. Lapidus IR, Welch M, Eisenbach M. 1988. Pausing of flagellar rotation is a component of bacterial motility and chemotaxis. *J Bacteriol* 170:3627–3632. <https://doi.org/10.1128/jb.170.8.3627-3632.1988>.
50. Armitage JP, Macnab RM. 1987. Unidirectional, intermittent rotation of the flagellum of *Rhodobacter sphaeroides*. *J Bacteriol* 169:514–518. <https://doi.org/10.1128/jb.169.2.514-518.1987>.
51. Qian C, Wong CC, Swarup S, Chiam K-H. 2013. Bacterial tethering analysis reveals a “run-reverse-turn” mechanism for *Pseudomonas* species motility. *Appl Environ Microbiol* 79:4734–4743. <https://doi.org/10.1128/AEM.01027-13>.
52. Eisenbach M, Wolf A, Welch M, Caplan SR, Lapidus IR, Macnab RM, Aloni H, Asher O. 1990. Pausing, switching and speed fluctuation of the bacterial flagellar motor and their relation to motility and chemotaxis. *J Mol Biol* 211:551–563. [https://doi.org/10.1016/0022-2836\(90\)90265-N](https://doi.org/10.1016/0022-2836(90)90265-N).
53. Kojima M, Kubo R, Yakushi T, Homma M, Kawagishi I. 2007. The bidirectional polar and unidirectional lateral flagellar motors of *Vibrio alginolyticus* are controlled by a single CheY species. *Mol Microbiol* 64:57–67. <https://doi.org/10.1111/j.1365-2958.2007.05623.x>.
54. Sourjik V, Schmitt R. 1996. Different roles of CheY1 and CheY2 in the chemotaxis of *Rhizobium meliloti*. *Mol Microbiol* 22:427–436. <https://doi.org/10.1046/j.1365-2958.1996.1291489.x>.
55. Bible A, Russell MH, Alexandre G. 2012. The *Azospirillum brasilense* Che1 chemotaxis pathway controls swimming velocity, which affects transient cell-to-cell clumping. *J Bacteriol* 194:3343–3355. <https://doi.org/10.1128/JB.00310-12>.
56. Kudo S, Imai N, Nishitoba M, Sugiyama S, Magariyama Y. 2005. Asymmetric swimming pattern of *Vibrio alginolyticus* cells with single polar flagella. *FEMS Microbiol Lett* 242:221–225. <https://doi.org/10.1016/j.femsle.2004.11.007>.
57. Morse M, Colin R, Wilson LG, Tang JX. 2016. The aerotactic response of *Caulobacter crescentus*. *Biophys J* 110:2076–2084. <https://doi.org/10.1016/j.bpj.2016.03.028>.
58. Freter R, O'Brien PC. 1981. Role of chemotaxis in the association of motile bacteria with intestinal mucosa: fitness and virulence of nonchemotactic *Vibrio cholerae* mutants in infant mice. *Infect Immun* 34:222–233. <https://doi.org/10.1128/iai.34.1.222-233.1981>.
59. Zhu S, Kojima S, Homma M. 2013. Structure, gene regulation and environmental response of flagella in *Vibrio*. *Front Microbiol* 4:410. <https://doi.org/10.3389/fmicb.2013.00410>.
60. Bubendorfer S, Koltai M, Rossmann F, Sourjik V, Thormann KM. 2014. Secondary bacterial flagellar system improves bacterial spreading by increasing the directional persistence of swimming. *Proc Natl Acad Sci U S A* 111:11485–11490. <https://doi.org/10.1073/pnas.1405820111>.
61. Saragosti J, Silberzan P, Buguin A. 2012. Modeling *E. coli* tumbles by rotational diffusion. Implications for chemotaxis. *PLoS One* 7:e35412. <https://doi.org/10.1371/journal.pone.0035412>.
62. Son K, Menolascina F, Stocker R. 2016. Speed-dependent chemotactic precision in marine bacteria. *Proc Natl Acad Sci U S A* 113:8624–8629. <https://doi.org/10.1073/pnas.1602307113>.
63. Xie L, Lu C, Wu X-L. 2015. Marine bacterial chemoresponse to a stepwise chemoattractant stimulus. *Biophys J* 108:766–774. <https://doi.org/10.1016/j.bpj.2014.11.3479>.
64. Moisi M, Jenul C, Butler SM, New A, Tutz S, Reidl J, Klose KE, Camilli A, Schild S. 2009. A novel regulatory protein involved in motility of *Vibrio cholerae*. *J Bacteriol* 191:7027–7038. <https://doi.org/10.1128/JB.00948-09>.
65. Utada AS, Bennett RR, Fong JCN, Gibiansky ML, Yildiz FH, Golestanian R, Wong GCL. 2014. *Vibrio cholerae* use pili and flagella synergistically to effect motility switching and conditional surface attachment. *Nat Commun* 5:4913. <https://doi.org/10.1038/ncomms5913>.

66. Nishiyama S-I, Takahashi Y, Yamamoto K, Suzuki D, Itoh Y, Sumita K, Uchida Y, Homma M, Imada K, Kawagishi I. 2016. Identification of a *Vibrio cholerae* chemoreceptor that senses taurine and amino acids as attractants. *Sci Rep* 6:20866. <https://doi.org/10.1038/srep20866>.
67. Nhu, NTQ, Lee JS, Wang HJ, Dufour YS. 2021. Alkaline pH increases swimming speed and facilitates mucus penetration for *Vibrio cholerae*. *J Bacteriol* 203: e00607–20. <https://doi.org/10.1128/JB.00607-20>.
68. Boyd S, Parikh N, Chu E, Peleato B, Eckstein J. 2010. Distributed optimization and statistical learning via the alternating direction method of multipliers. *FnT Mach Learn* 3:1–122. <https://doi.org/10.1561/22000000016>.
69. Frenkel ES, Ribbeck K. 2015. Salivary mucins protect surfaces from colonization by cariogenic bacteria. *Appl Environ Microbiol* 81:332–338. <https://doi.org/10.1128/AEM.02573-14>.
70. Degnen ST, Newton A. 1972. Chromosome replication during development in *Caulobacter crescentus*. *J Mol Biol* 64:671–680. [https://doi.org/10.1016/0022-2836\(72\)90090-3](https://doi.org/10.1016/0022-2836(72)90090-3).
71. Grognot M, Mittal A, Mah'moud MA, Taute KM. 2021. 3D trajectory data and code for *Vibrio cholerae* motility in aquatic and mucus-mimicking environments. Harvard Dataverse <https://doi.org/10.7910/DVN/FNWZ2Q>.